Influence of the overall stiffness of a load-bearing porous titanium implant on bone ingrowth in critical-size mandibular bone defects in sheep

T. Schouman[a,b,*], *M. Schmitt*[b,c], *C. Adam*[d], *G. Dubois*[b,c], *P. Rouch*[b]

[a]*APHP-Pitie Salpetriere University Hospital, Department of Oral and Maxillofacial Surgery, Paris, France*
[b]*Arts et Metiers ParisTech, LBM/Institut de Biomecanique Humaine Georges Charpak, Paris, France*
[c]*OBL, Chatillon, France*
[d]*Paediatric Spine Research Group, School of Chemistry, Physics and Mechanical Engineering, Faculty of Science and Engineering, Queensland University of Technology, Brisbane, Australia*

Keywords:
Bone substitute
Porous titanium scaffold
Bone tissue engineering
Mandibular reconstruction
Large animal model
Sheep

A B S T R A C T

The aim of this work was to assess the influence of reduction of the apparent mechanical properties of fully load-bearing porous titanium implants used in mandibular bone defects.

Segmental 18 mm long bone defects were created bilaterally in the lower jaws of adult ewes. One group of 6 ewes (group A) was treated with load-bearing 'rigid' (high stiffness) porous implants on the right side, and with control on the left side. A second group of 6 ewes (group B) was treated with 'flexible' porous and control implants exhibiting apparent mechanical properties ten times lower than the rigid implants. The mechanical behavior of the reconstructed hemi-mandibles was assessed by cantilever testing and bone ingrowth into the segmental defects was assessed by BV/TV measurement within the implant using micro-CT 12 weeks after implantation.

A significantly higher rigidity was identified for porous implants compared with control implants at the anterior interface in group B. BV/TV of porous implants was significantly higher than that of control implants in group A. BV/TV differences were significant between porous and control implants in group B and were homogeneous along the main axis. Significantly higher BV/TV was identified in most sub-volumes of group B porous implants compared with group A.

This work highlights the critical importance of the tuning of scaffolds to promote bone ingrowth with reference to the local strains occurring within the porous scaffold, which in this application was achieved using fully load-bearing low-stiffness porous titanium implants.

1. Introduction

Bone defects of the lower jaw present significant challenges in maxillo-facial reconstruction. Autologous non vascularized bone grafts are usually recommended for the reconstruction of defects smaller than 5 cm with a favorable soft tissue environment providing sufficient blood supply (Goh et al., 2008). However, the rate of failure is highly dependent on the stability of bone fixation and can exceed 50% (Foster et al., 1999). For larger defects, or when the defect involves the surrounding soft tissue, bone flap surgery is needed (Mehta and Deschler, 2004). This procedure is considered the gold standard for lower jaw reconstruction with reported success rates over 90% (Goh et al., 2008). Both surgical techniques involve autograft harvest from a healthy donor site and possible related complications, and the amount of bone that can be harvested is limited (Myeroff and Archdeacon, 2011; Momoh et al., 2011; Catalá-Lehnen et al., 2012; Kerrary et al., 2011). The shaping of such bone grafts or transplants to adapt them to the contour of the missing bone segments can be challenging without risking damage to the flap's pedicle or instability of the graft. Surgical navigation or custom surgical guides can help increase the accuracy of the reconstruction (Bell et al., 2011; Hirsch et al., 2009; Schouman et al., 2015).

Tissue engineering approaches in such cases aim at obtaining bone growth into scaffolds mimicking bone micro-architecture. The use of pre-shaped scaffolds could radically change existing surgical approaches to bone defect reconstruction, since no autologous bone would need to be harvested and shaped. Integration into surrounding tissue and osteoconduction could be achieved by mimicking the morphological, structural and functional features of the missing segment (Karageorgiou and Kaplan, 2005). The critical role of porosity and pore size in bone regeneration, as well as that of the mechanical properties of porous implants have been investigated over the last two decades (Karageorgiou and Kaplan, 2005; Otsuki et al., 2006 Dec; Xue et al., 2007). However, prior studies have often not distinguished between implants made of a porous structure intended to function as scaffolds, and solid implants with a porous cortex or surface roughness intended to promote osseointegration. Porous implants are usually made of ceramics (mainly hydroxyapatite), metals or polymers. Ceramic brittleness is the main disadvantage of this material despite its osteogenic ability (Drosos et al., 2012). Polymers have limited strength and stiffness and therefore can only be used in bone sites with low levels of stress. Polymer/ceramic composites exhibit limited strength ranging from 2 to 10 MPa, which is in the low to middle range for human trabecular bone (Hollister et al., 2005). Metallic implants, specifically titanium porous implants, are better suited to the surgical repair of bone defects in highly loaded anatomical sites because of their excellent mechanical properties (Karageorgiou and Kaplan, 2005; Barbas et al., 2012; He et al., 2013; He et al., 2012; Oh et al., 2003; St-Pierre et al., 2005). The pore size of metallic scaffolds in prior studies has ranged from less than 100 μm to 1500 μm, and the porosity from 13 to 86% (Karageorgiou and Kaplan, 2005; Otsuki et al., 2006 Dec; Barbas et al., 2012). According to Karageorgiou and Kaplan (2005), higher porosity and pore size allow for better bone ingrowth. However, increased porosity and pore size implies reduction of the mechanical strength and stiffness that can be critical for the reconstruction of load-bearing bones. Sintering or melting of titanium powders allows 3D-printing of complex structures, including porous structures with precisely controlled micro-architecture (Barbas et al., 2012; Marin et al., 2013; Otawa et al., 2015). The scaffold can thus be designed to replicate the outer shape of the missing bone and its mechanical response can be adapted to the functional loading. Marin et al. (2013) tested two types of porous implants obtained by electron beam melting (EBM) of grade 2 titanium powders. Their trabecular titanium implant with pores of 1250 μm exhibited a low elastic modulus comparable to that of human trabecular bone and much less than that of cortical bone. The titanium scaffold microarchitecture developed by Barbas et al. (2012) conferred mechanical properties slightly superior to those of human femoral cortical bone.

Aside from the direct influence of pore size, pore interconnection and porosity on bone ingrowth, the role of the overall apparent mechanical properties (stiffness and strength) of the implant on bone formation remains insufficiently explored. In the field of fracture treatment, excess rigidity of implants as compared to the host bone is a well-known cause of implant failure. The stress shielding effect resulting from the rigidity discrepancy can induce bone resorption in some regions around the implant that are no longer subject to significant stress. Therefore, it is recommended to use implants exhibiting Young's moduli similar to that of the host bone (Niinomi and Nakai, 2011). Furthermore, the local stresses and strains transmitted within rigid porous implants under mechanical loading can be inadequate to induce the desired cell proliferation and differentiation to obtain bone formation, regardless of the micro-architectural parameters (porosity, pore size and pore interconnection). More precisely, we question the capability of a porous scaffold exhibiting mechanical properties equal or higher to that of cortical bone to provide adequate mechanical signals for the successful regeneration of bone tissue into its pores. We note that previous authors have also hypothesized that reduced stiffness (allowing greater deformation of porous implants under load) could result in improved bone ingrowth (Van der Stok et al., 2013; Wieding et al., 2015).

The aim of this study was to assess the influence of the rigidity of titanium porous implants used for the reconstruction of lower-jaw defects on bone ingrowth. To this end, we designed an experimental study in sheep to compare bone formation into porous implants with two different rigidities. Bone ingrowth was assessed by post-sacrifice mechanical testing of implanted mandibles and by measurement of the volume of newly formed bone using micro-CT scans.

2. Materials and methods

2.1. *Implant design*

The ovine mandibular arch encompasses an anterior portion bearing incisors, bilateral posterior regions bearing premolars

and molars, and bilateral intermediate tooth-free segments mainly composed of cortical bone (Fig. 1). An 18-mm long bone defect within the edentulous segment (i.e. intermediate part) of sheep mandibles was performed bilaterally. The bone defect presented a tubular shape, which could be represented as a section of a cone aligned along the main axis of the mandibular corpus.

A first implant (rigid porous implant) corresponding in external dimensions to the planned bone defect on the right side was created using an existing porous titanium implant design (PorousiTi®, OBL, Châtillon, France). Rigid bone-fixation lugs extending from the implant were designed at each end of the implant (Fig. 2a). The properties of this porous implant were described by Barbas et al. (2012): the porosity is 53%, and the size of the pores ranges from 800 μm to 1500 μm; its anisotropic behavior is characterized by an apparent (overall) modulus of elasticity E_1 of 37.9 GPa for the first direction (longitudinal), and E_2=18 GPa and E_3=15.8 GPa for the second and third directions (elliptical cross-section long and short axes, respectively). A hollow control implant of equal stiffness (rigid control implant) acting like a periosteal tent was designed to stabilize the bone ends and to maintain the spacing of the bone defect on the left side in an identical manner to the rigid porous implant (Fig. 2b). A third implant with reduced stiffness (flexible porous implant) was developed to fit in the right-side bone defect. In this reduced stiffness implant, slices replicating the same repeated 'asterisk' internal strut pattern as used in the current PorousiTi® implant were aligned perpendicularly to the main axis of the cone section and were joined by a lateral beam (Fig. 2c). The dimensions of the beam were calculated to obtain a stiffness ten times lower than that of the rigid porous implant. The corresponding hollow control implant (flexible control implant) on the left side again consisted of a periosteal tent with the same reduced flexural rigidity as the contralateral porous implant. In this low stiffness control implant,

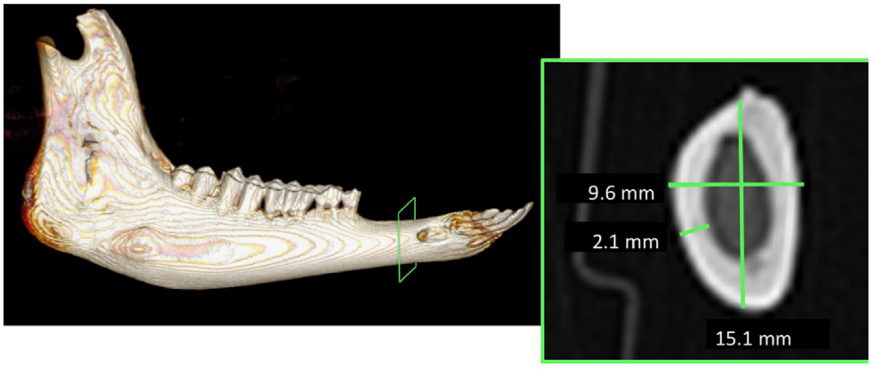

Fig. 1 – Medical CT scan of an ovine mandible. 3D reconstruction and zoomed-in axial section showing the geometry of the edentulous segment between posterior and anterior parts of the mandibular arch used as the implantation site.

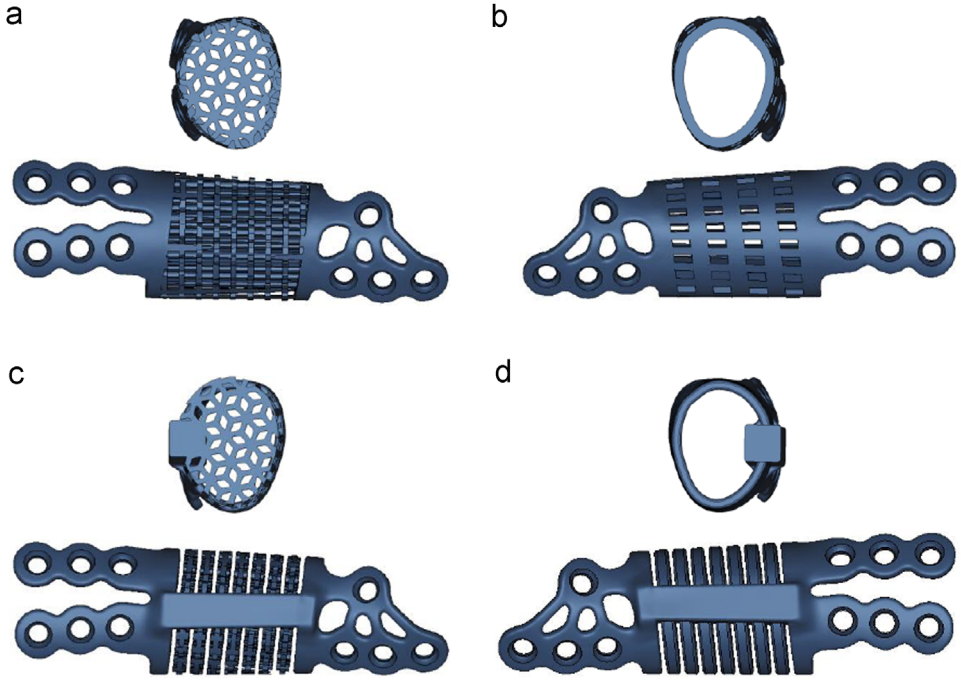

Fig. 2 – Lateral and transverse views of each implant type: (a) rigid porous implant, (b) rigid control implant, (c) flexible porous implant and (d) flexible control implant.

continuous rings of Ti void of porous structure were fixed to the same lateral beam (Fig. 2d). The overall implant dimensions and fixation plates remained the same for all four implants. All implants were produced by additive manufacturing using selective laser melting of surgical grade 2 titanium powder, and were further anodized prior to sterilization.

2.2. *Experimental design*

2.2.1. *Study design*

The Institutional Ethical Committee for Animal Experimentation approved the study (CEEA34.TS.155.12). Twelve adult ewes (more than 12 months of age) were divided in two groups of six. A rigid porous implant was implanted on the right hemi-mandible and the corresponding control implant on the left side in each ewe of group A. Group B received a flexible porous implant on the right side and a flexible control implant on the left side.

2.2.2. *Animal experiment*

After premedication, 4 mg/kg of intravenous Propofol was administered for the induction of anesthesia. An endotracheal tube was placed and Isoflurane with 100% oxygen inhalation was used for anesthesia maintenance. The ewes were positioned on the operating table lying supine and the submental region was shaved (i.e. the neck region located under the chin). The surgical site was prepared aseptically. A V-shaped submental incision was performed, the periosteum was elevated along both mandibular corpuses and the symphyseal region (lateral and anterior portions). A 2.5 mm thick titanium plate with monocortical screws temporarily bridged mandibular angles in order to stabilize the bone segments of the mandible during bone resection. The following procedure was repeated on each side successively: the 18 mm long implant was used as a template to mark the edges of the corresponding bone defect to create in the edentulous segment of the mandibular corpus, between the incisors and molars. The mandibular corpus was transected orthogonally at the proximal and distal marks using a reciprocating saw and the bone was removed, taking care not to cause any damage to the superior aspect of the periosteum in close contact with oral mucosa. The implant was fitted into the bone defect aiming at maximal contact between each bone end and the implant, and between implant lugs and the bone surface. Pilot screw holes were drilled under continuous irrigation. Three bicortical and 3 monocortical screws (the closest to the dental roots) were used for the posterior fixation and 4 bicortical screws were used for the anterior fixation (Fig. 3).

The periosteum and skin were closed using absorbable sutures. The endotracheal tube was removed once spontaneous breathing was recovered. Analgesia was continued for the next 3 days using morphine hydrochloride (0.05–0.5 mg/kg). 2 mg/kg/day of Ketoprofen and 750 mg of Cefamandole per day were administered during the next 5 days. Ewes were sacrificed 12 weeks later by lethal intravenous injection of pentobarbital 1 mg/kg. The mandible was collected, and split along the symphyseal line. The excised hemi-mandibles were fixed for 30 days in a 10% phosphate-buffered formaldehyde solution.

2.2.3. *Plain X-ray*

The specimens were radiographed using a high density digital X-ray to identify implant fracture and screw loosening. Radiographic assessment of the osseointegration of the cortical screws described anterior and posterior bone fixation stability. The screw-bone contact was ranked on a 3-grade scale as follows: 0=loosening of most screws, 1=limited bone resorption around some screws, 2=satisfactory osseointegration of the fixation screws. The integrity of the anterior and posterior implant-fixation lugs was similarly ranked as 0 for complete fracture causing loss of continuity between the implant and bone, 1 for incomplete fracture with preserved continuity, and 2 for perfect integrity. These rankings were further cross-referenced with micro-CT results. Two independent observers conducted the ranking once. In case of ranking discrepancy, the two observers reviewed the images together to determine an agreement.

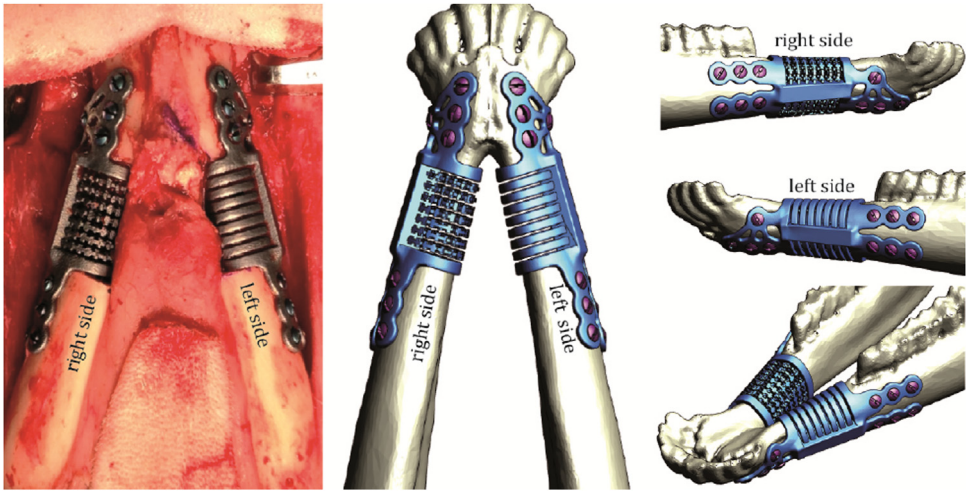

Fig. 3 – Operative downward view of the mandible of a group-B ewe equipped with the porous implant on the right side and the control implant on the left side.

2.2.4. *Mechanical testing*

Each hemi-mandible explant was subjected to a cantilever-bending test using a universal testing machine (INSTRON 5500-R, Norwood, MA, United States). A black and white speckle pattern coating was applied to the specimen using aerosol spray paint. The proximal segment of the mandible (i.e. ramus) was embedded into poly-methyl-methacrylate (PMMA) leaving 9 cm of the distal mandible protruding, positioned in the same orientation as would occur in vivo. The embedded hemi-mandible was then mounted on an x-y bearing plate (to prevent the generation of lateral forces) and the incisors were loaded with a cylinder nose indenter at 2 mm/min vertical downward displacement until reaching a moment of 6 N m in the ramus (Fig. 4). The resultant force was recorded using a 1000 N INSTRON load cell at an acquisition rate of 10 kHz. Frontal images of the setup were captured every two seconds using a fixed digital camera for Digital Image Correlation (DIC). A fixed 100-point correlation grid was positioned along the main axis of the mandible on the lateral view at $t=0$ as shown in Fig. 4. The DIC grid was further tracked in the image series by means of 2D-image registration using MATLAB and Statistics Toolbox (Release 2012b, The MathWorks, Inc., Natick, Massachusetts, United States). The deflection curve as obtained from the grid deformation at the end of the loading (i.e. 6 N m) was used to assess the rigidity of the anterior and posterior bone–implant interfaces. In order to calculate the deflection, the raw displacement field obtained from the DIC was smoothed using a three point moving average filter. The mean gradients of the displacement curves proximally and distally to each interface were calculated using numerical differentiation on a five-point stencil. The condition of each interface was then quantitatively assessed using the ratio of the proximal deflection curve gradient to the distal gradient, such that an interface gradient ratio of 100% (no change in gradient across the interface) corresponds to a perfectly rigid interface and 0% corresponds to a broken interface. All rigidity ratio calculations were performed at 33 N applied force which provided sufficient displacement for good DIC resolution while maintaining the mandibles in the elastic regime. This force corresponded to 2 N m moment at the posterior interface and 1.4 N m moment at the anterior interface. The same protocol was used to assess the mechanical behavior of two healthy (i.e. unoperated) hemi-mandibles, which were also fixed in the 10% phosphate-buffered formaldehyde solution prior to mechanical testing. The first one was left unchanged and the second was tested after creation of a bone defect and placement of a rigid porous implant to obtain reference deflection curves (i.e. healthy hemi-mandible and implanted hemi-mandible at $t=0$).

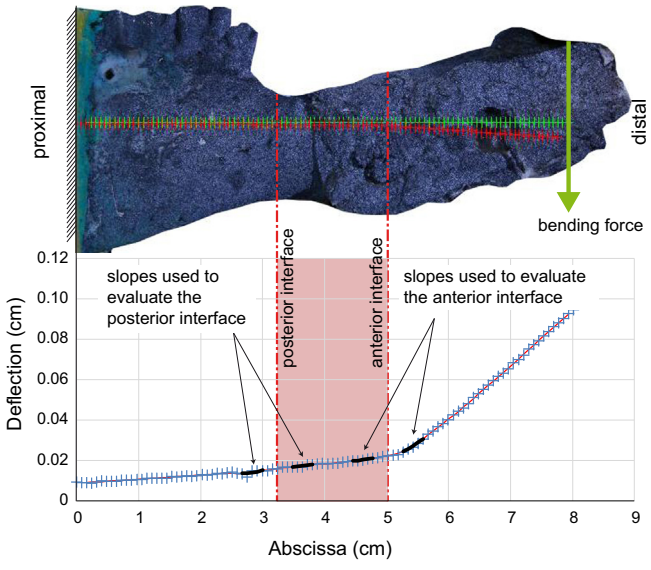

Fig. 4 – Calculation of the gradients proximal and distal to each interface to characterize the rigidity of the anterior and posterior interfaces.

Statistical analyses were performed using XLSTAT (Addinsoft, Paris, France). The median, interquartile, and range of stiffness ratio were calculated in each group. The differences between rigid porous versus control implants, flexible porous versus control implants, porous rigid versus flexible implants and control rigid versus flexible implants were compared for both the anterior and posterior interfaces. The Mann-Whitney test was used to analyze the differences between the groups. *P*-values <0.05 were considered significant.

2.2.5. *Micro-CT scan*

Implants including at least 5 mm of protruding bone at each end were excised from the mandible. The specimens were placed obliquely into a 7 cm diameter specimen holder and a micro-CT scan (SCANCO μCT 100, Brüttisellen, Switzerland) was performed on each implant as follows: tube voltage-70 kV, current-114 μA, integration time-1500 ms. The resulting voxel size was 36.8 μm.

Post-processing of μCT images was performed using Mimics 15.01 and 3-Matic 7.01 (Materialise, Leuven, Belgium). DICOM files were imported into Mimics. Segmentation of titanium and bone was achieved by selecting (16 bit) gray scales between 3900 and 22,000 for bone (as determined visually for mandibular native bone in regions free of titanium), and between 22,000 and 32,760 (maximum value) for titanium. Segmentation of titanium was dilated by 3 pixels to remove the artifacts in the immediate vicinity of the titanium (in red on Fig. 5). A mask corresponding to the volume of the bone defect was created in 3-matic by generating a shell around the implant body. This volume was divided into several sub-volumes: (i) 3 slices of equal thickness along the main axis (named P for the posterior, I for intermediate, and A for anterior) and (ii) a central longitudinal cylinder of 3 mm diameter (named CC) *vs* the remaining peripheral annular volume (named PP) (Fig. 6). For each sub-volume, the total volume (TV) available for bone ingrowth was calculated by a Boolean subtraction of dilated titanium from sub-volume. The volume of newly formed bone in each sub-volume of the implant (Bone Volume, BV) was obtained by a Boolean intersection between bone and the corresponding sub-volume. The volume of newly formed bone included in the bone defect (Total Bone Volume, TBV) was measured by calculating the bone volume included between the planes aligned with the proximal and distal edges of the bone defect.

One empty sample of each implant was positioned in the μCT specimen holder at varying angulations to the X-ray beam from 20° to 70° to assess the amount of titanium-

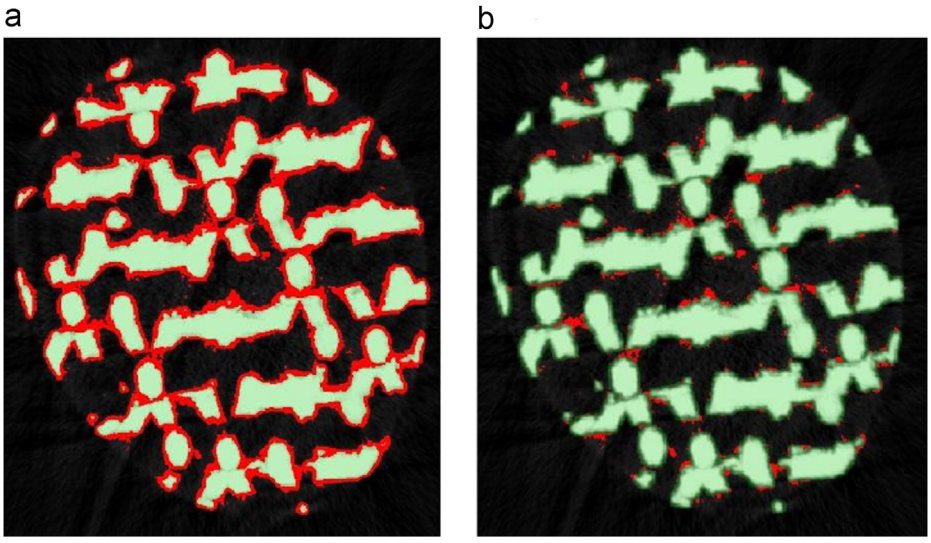

Fig. 5 – Micro-CT images of an empty porous implant showing the segmentation of the titanium before (a) and after the 3-pixel dilation to mask the bordering artifacts (b). Pixels corresponding to titanium gray levels are in green, pixels corresponding to bone tissue gray levels (i.e. implant artifacts) are in red. The 3-pixel dilation succeeds in removing nearly all the low gray level artefact due to partial volume averaging. (For interpretation of the references to color in this figure legend, the reader is referred to the web version of this article.)

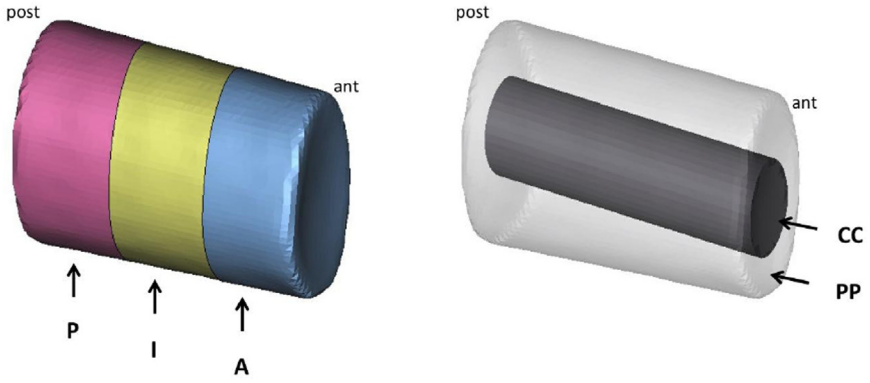

Fig. 6 – Division of the total implant volume into 3 longitudinal subvolumes (anterior: A, intermediate: I, posterior: P) and two concentric subvolumes (central: CC, peripheral: PP).

related artifact as a function of implant orientation in the scanner. The DICOM data were post-treated using the above-described procedure to calculate the BV, TV and TBV specifically generated by the artifacts.

Statistical analyses were performed using XLSTAT (Addinsoft, Paris, France). The median, interquartile, and range of BV/TV for each sub-volume were calculated. The BV/TV differences between the porous implant and control implant were compared between group A and group B. A 'worst-case' study was further conducted using the same comparisons of porous *vs* control implants after subtraction of the artifact-related BV/TV as obtained from the empty implant assessment in the porous-implant only. The BV/TV of the porous implants of group A *vs* group B were compared, as well as that of the control implants. The Mann-Whitney test was used to analyze the differences between the groups. *P*-values <0.05 were considered significant.

3. Results

3.1. *Animal experiment*

One ewe from group B was sacrificed 2 weeks after surgery due to implant fracture and exposure with local infection. The 12-week post-operative period was uneventful for all other ewes, including normal oral feeding.

3.2. *Plain X-ray*

Only 1 implant fixation lug fracture occurred at the posterior end in group A, on the porous implant side, whereas screw loosening was frequently identified, mainly at the anterior end (Table 1). In group B, implant lug fractures were

Table 1 – Percentages of implants per grade in each group describing the osseointegration of the cortical screws and the integrity of the implant fixation lugs. (Screw grades: 0=loosening of most screws, 1=limited bone resorption around some screws, 2=satisfactory osseointegration. Fixation lugs grade: 0=complete fracture, 1=incomplete fracture with preserved continuity, and 2=perfect integrity.)

	Grade	Porous implant				Control implant			
		Anterior screws	Posterior screws	Anterior lugs	Posterior lugs	Anterior screws	Posterior screws	Anterior lugs	Posterior lugs
Group A	0	50%	–	–	–	17%	–	–	–
(n=6)	1	33%	66%	–	17%	50%	17%	–	–
	2	17%	33%	100%	83%	33%	83%	100%	100%
Group B	0	–	–	–	60%	–	–	–	80%
(n=5)	1	40%	–	–	20%	–	–	20%	20%
	2	60%	100%	100%	20%	100%	100%	80%	–

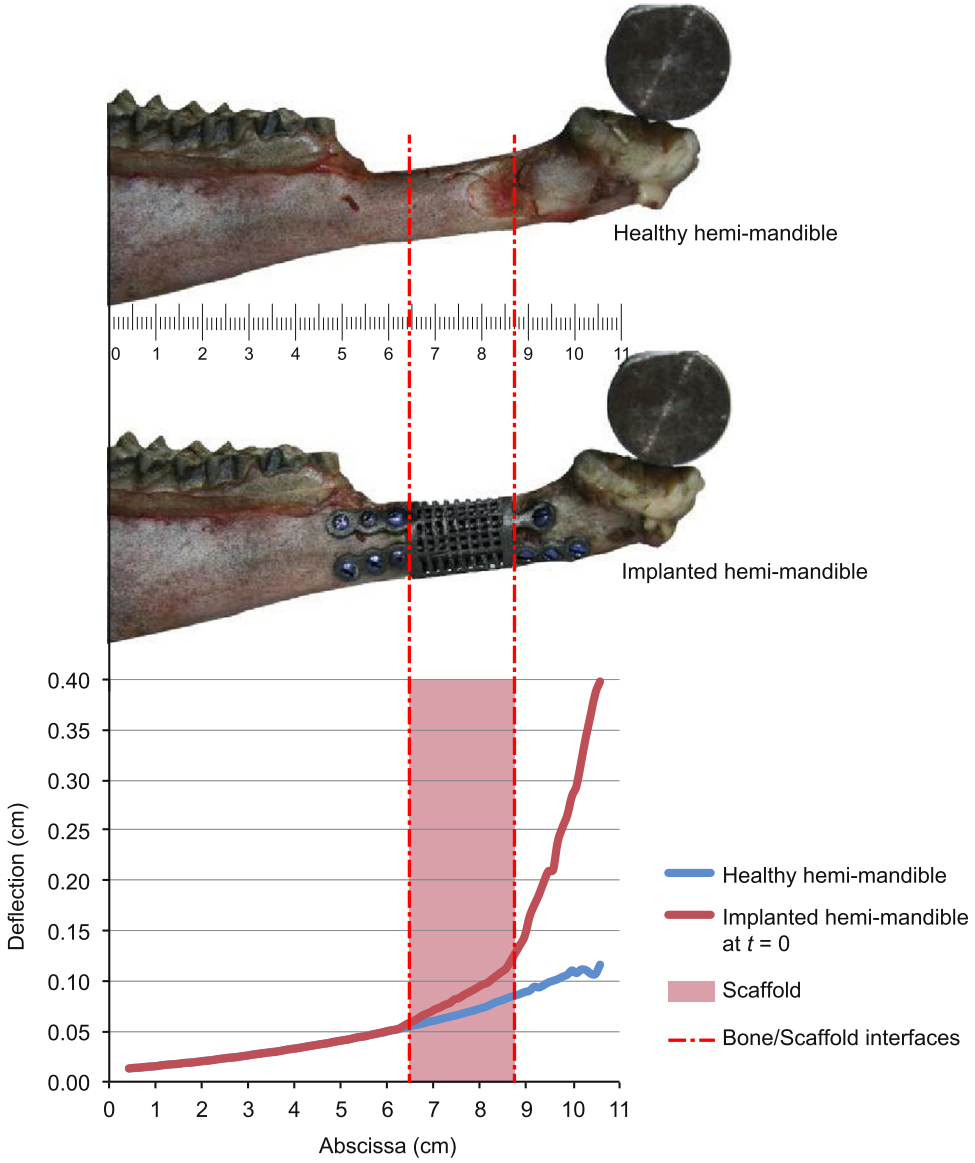

Fig. 7 – Deflection curves of a non-implanted hemi-mandible exhibiting continuous deflection along the main axis (blue curve) and of the same hemi-mandible after segmental bone resection and insertion of a rigid porous implant (red curve) at t=0 (i.e. without any bone colonization of the interfaces). Note the identical deflection in the proximal segment (0–6.5 cm) and the two hinge points in the implanted mandible at 6.5 cm and 9 cm corresponding to the two bone–implant interfaces. (For interpretation of the references to color in this figure legend, the reader is referred to the web version of this article.)

frequently found at the posterior end, whereas screw loosening was infrequent (Table 1).

3.3. *Mechanical testing*

As expected, the healthy hemi-mandible demonstrated a continuous deflection curve along the axis of the mandible from the embedded point to the distal tip. Testing of the implanted hemi-mandible at $t=0$ demonstrated two deflection curve gradient discontinuities corresponding to the'-hinge points' at the bone–implant interfaces. The posterior and anterior bone–implant interfaces were characterized by interface gradient ratios of 40% and 15% respectively (Fig. 7).

In group A (Fig. 8a), no significant difference was found between porous and control implants though porous implants exhibited a clear tendency toward higher interfacial rigidity at both the posterior and anterior interfaces, close to the maximum at the posterior interface (Fig. 9a). In group B (Fig. 8b), a significantly higher interface rigidity was identified for porous implants compared with controls at the anterior interface ($p=0.016$), with porous implants exhibiting ratios close to the maximum. This difference was not significant at the posterior interface despite an overall higher interface rigidity ratio, close to the maximum, for porous implants compared with controls (Fig. 9b). When considering porous implants alone, the interface rigidity ratios were comparable and close to the maximum for both rigid and flexible implants at the posterior interface, and clearly but not significantly lower for rigid implants at the anterior interface compared with flexible implants (Fig. 9c). Considering control implants alone, no difference was identified either at the anterior nor posterior interface between rigid and flexible implants, with anterior interfaces tending to a lower rigidity ratio than posterior interfaces in both groups (Fig. 9d).

3.4. *Micro-CT scan*

The BV/TV measured in empty porous implants, either rigid or flexible, caused due to artifact was 7.5%. This value varied from 6% to 9% depending on the angulation between the implant and the X-ray beam. The artefactual BV/TV was around 1.7% for the hollow control implants, ranging from 0.7% to 2%.

In group A, the BV/TV of porous implants was significantly higher than that of control implants in sub-volumes I and A ($p=0.013$ and $p=0.045$, respectively) (Figs. 10 and 11). Although it was not significant, BV/TV seemed to decrease from the posterior to the anterior end of the bone defect for both implants. The comparison of BV/TV in the central and peripheral sub-volumes of the porous implant showed no significant difference ($p=0.936$) whereas bone ingrowth of the control implant was significantly higher in the peripheral region ($p=0.045$). These differences were no longer significant

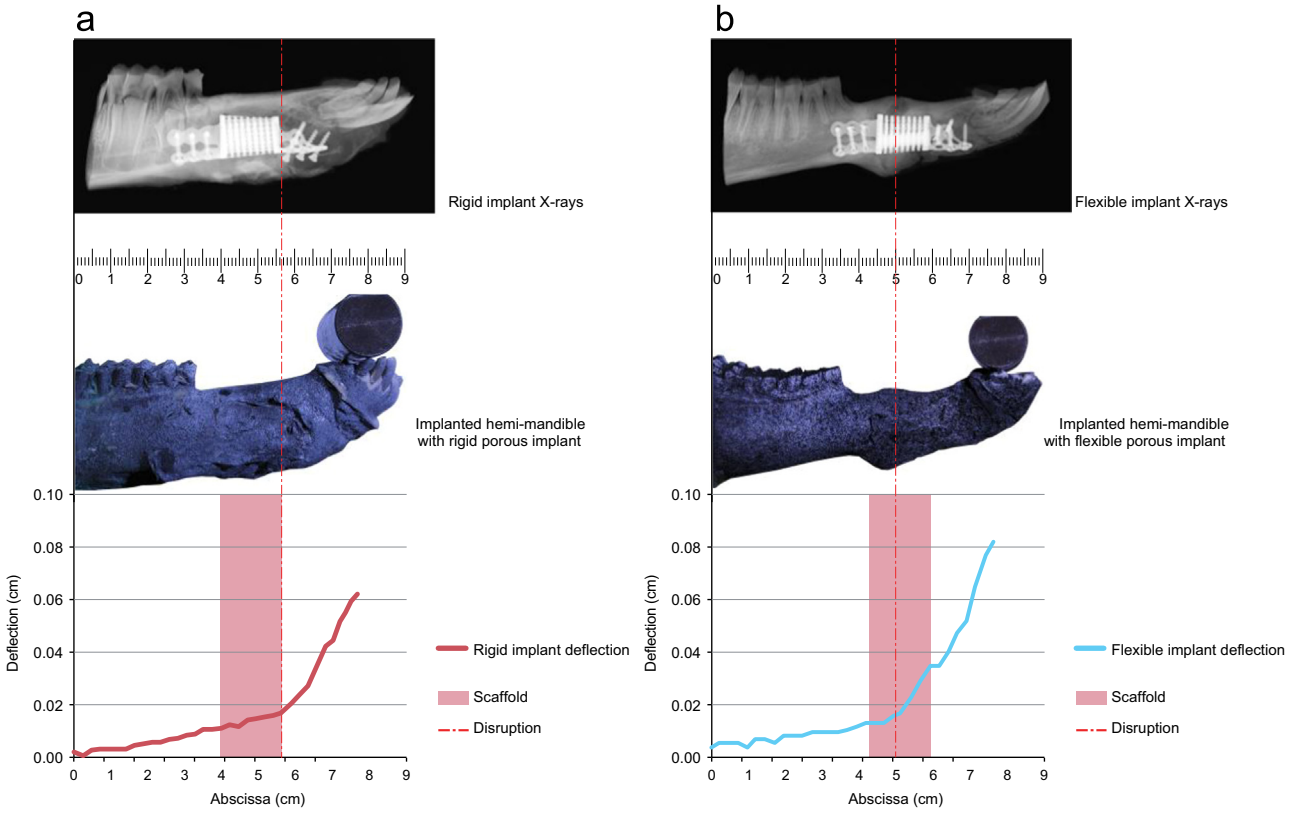

Fig. 8 – (a) Deflection curve of a right hemi-mandible of group A (rigid porous implant) with typical deflection curve gradient discontinuity (hinge point) corresponding to the anterior bone–implant interface. (b) Deflection curve of a right hemi-mandible of group B (flexible porous implants) with typical hinge point within the span of the implant.

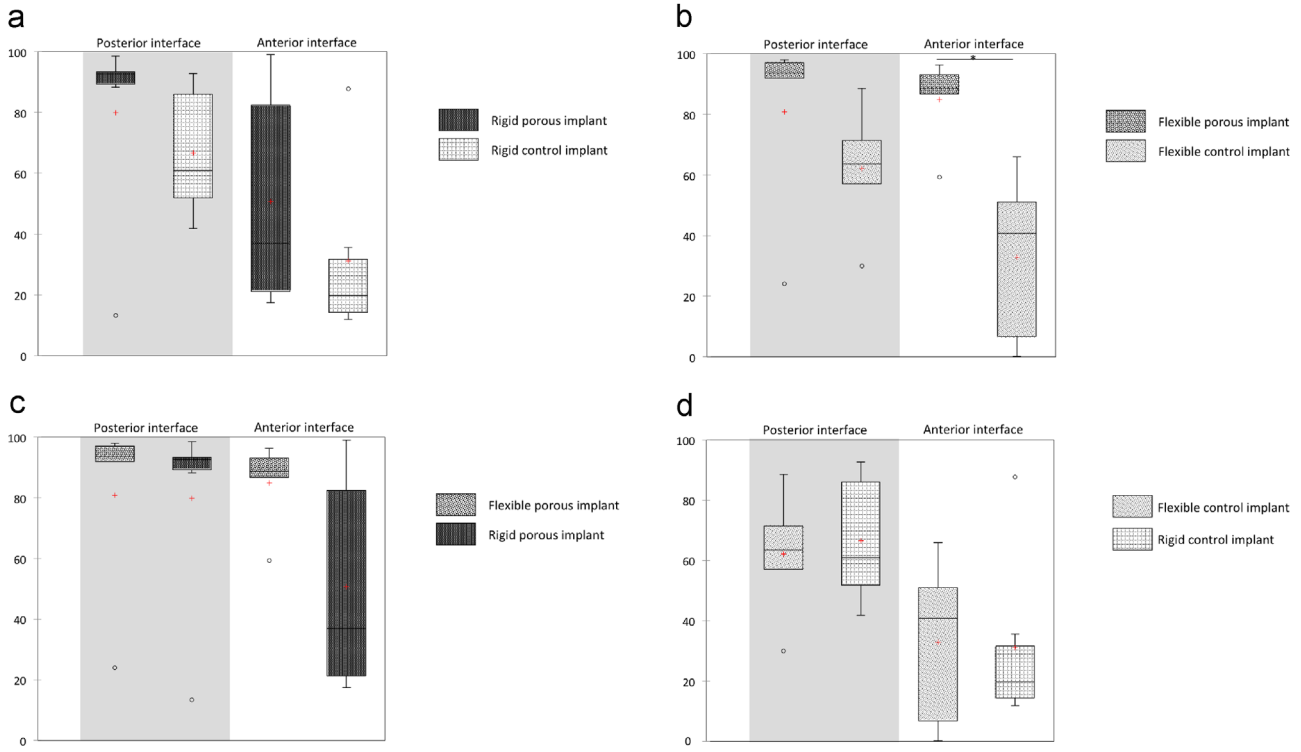

Fig. 9 – (a) Group A rigidity ratios for porous *vs* control implants at the anterior and posterior interfaces (red crosses are the means). (b) Group B rigidity ratios for porous *vs* control implants at the anterior and posterior interfaces (red crosses are the means, $^{*}p<0.05$). (c) Porous implant rigidity ratios for group A *vs* group B implants at the anterior and posterior interfaces (red crosses are the means). (d) Control implant rigidity ratios for group A *vs* group B implants at the anterior and posterior interfaces (red crosses are means). (For interpretation of the references to color in this figure legend, the reader is referred to the web version of this article.)

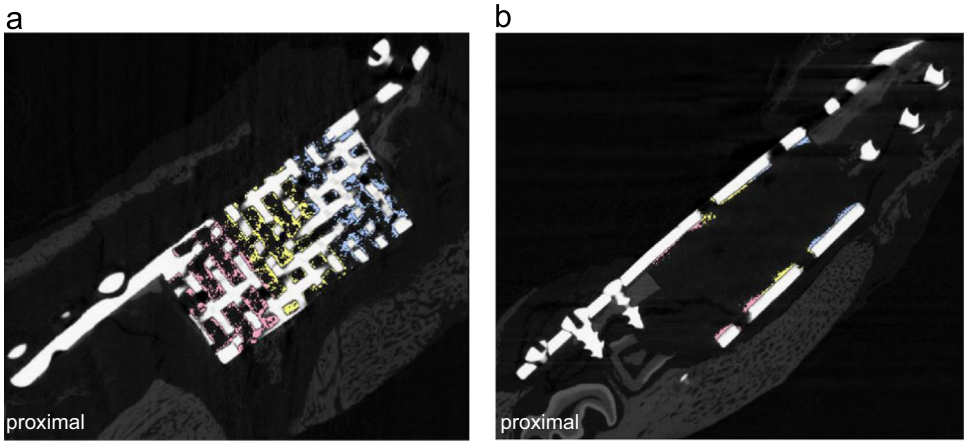

Fig. 10 – BV segmentation for each sub-volume (anterior (A) is in blue, intermediate (I) is in yellow, posterior (P) is in pink) in porous (a) and control (b) implants of group A. (For interpretation of the references to color in this figure legend, the reader is referred to the web version of this article.)

in the worst-case (potential artefact effects removed from BV/TV calculation) scenario.

Concerning group B, the BV/TV in the porous implants was significantly higher than that in the control implants in all three sub-volumes P, I and A ($p=0.022$, $p=0.008$, and $p=0.022$, respectively) (Figs. 12 and 13). There were comparable volumes of bone regenerated along the three longitudinal thirds of the implant in both porous and control implants (Fig. 10). No significant difference between the BV/TV of the central and peripheral sub-volumes was identified for both

implants. In the worst-case scenario, significant differences were still present for the total BV/TV ($p=0.037$), and for sub-volumes I ($p=0.022$), CC ($p=0.022$) and PP ($p=0.037$).

The comparison of BV/TV between rigid and flexible implants demonstrated a significant difference in favor of flexible implants in region I ($p=0.014$) and in region A ($p=0.004$) for porous implants (Fig. 14). Peripheral BV/TV and central BV/TV were both significantly higher in flexible porous implants ($p=0.014$ and $p=0.004$ respectively) compared with rigid.

With regard to the control implants, flexible implant BV/TV was significantly higher only in the anterior third ($p=0.036$) (Fig. 15). No significant difference was found between the two groups with regards to central and peripheral BV/TV.

4. Discussion

Porous titanium implants mimicking bone tissue microarchitecture and mechanical behavior have several advantages that could help reconstruct segmental defects in bone (Karageorgiou and Kaplan, 2005), particularly for applications where immediate mechanical resistance to high loads is required. This study aimed at determining the influence of the overall stiffness of fully load-bearing porous titanium implants on the regeneration of bone tissue into the implant pores. Our results demonstrate that tuning the overall stiffness of such implants can promote bone ingrowth in critical-size defects of the lower jaw in adult ewes.

To our knowledge, this study is the first to assess bone ingrowth of porous titanium implants bearing all the functional load of the missing bone segment. Among previous

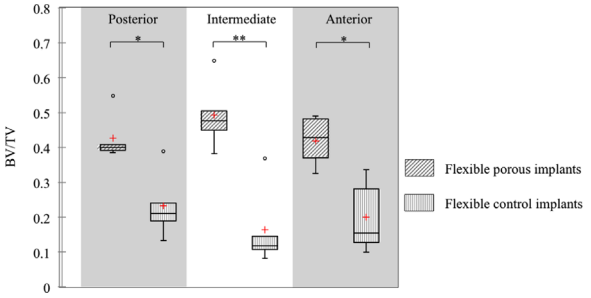

Fig. 13 – BV/TV of porous implants versus control implants of group B in the three longitudinal thirds (sub-volumes P, I and A) (red crosses are the means, $^{*}p<0.05$, $^{**}p<0.01$). (For interpretation of the references to color in this figure legend, the reader is referred to the web version of this article.)

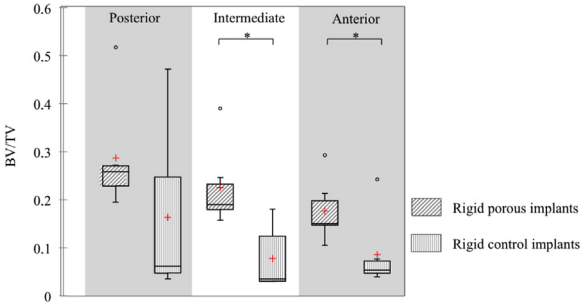

Fig. 11 – BV/TV of porous implants versus control implants of group A in the three longitudinal thirds (sub-volumes P, I and A) (red crosses are the means, $^{*}p<0.05$). (For interpretation of the references to color in this figure legend, the reader is referred to the web version of this article.)

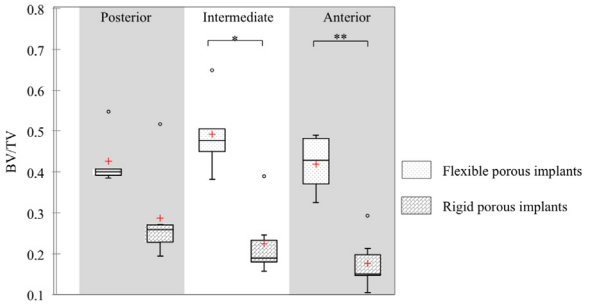

Fig. 14 – BV/TV of group A versus group B porous implants in the three longitudinal thirds (sub-volumes P, I and A) (red crosses are the means, $^{*}p<0.05$, $^{**}p<0.01$). (For interpretation of the references to color in this figure legend, the reader is referred to the web version of this article.)

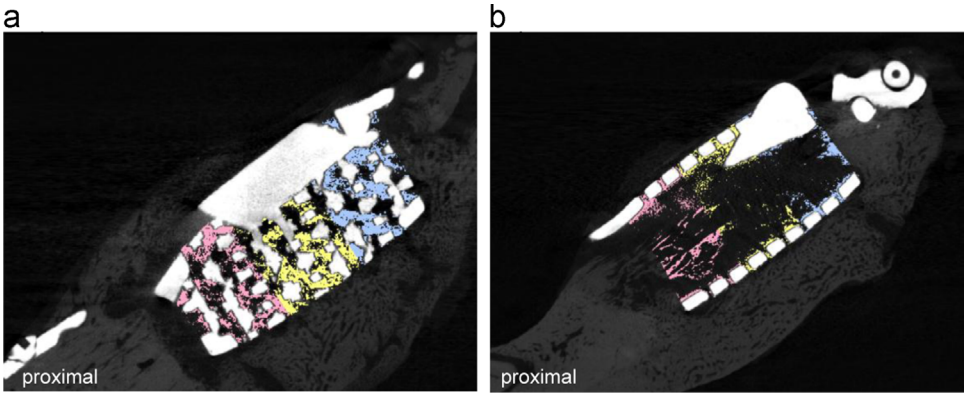

Fig. 12 – BV segmentation for each sub-volume in porous (a) and control (b) implants of group B.

studies addressing the issue of bone ingrowth of porous titanium implants, some assessed the performance of the porous implant used *in vitro* as a scaffold for osteoblast cell culture (Xue et al., 2007; St-Pierre et al., 2005; Warnke et al., 2009; Lopez-Heredia et al., 2008) or after *in vivo* implantation into the soft tissue (Lopez-Heredia et al., 2008; Palmquist et al., 2013; Vehof et al., 2000, 2001; Fujibayashi et al., 2004), *i.e.* without mechanical loading of the implants. Porous implants inserted in non-interruptive bone defects were either not mechanically loaded (De Wild et al., 2013; Ponader et al., 2010) or were potentially subjected to marginal load levels when the bone of interest was located in the limb (Otsuki et al., 2006 Dec; Takemoto et al., 2005; Faria et al., 2010). Recently, Van der Stok et al. (2013) and Wieding et al. (2015) compared bone ingrowth of porous titanium implants placed in interruptive bone defects of the limb of rats and sheep respectively, which implied implant loading. However, in both studies, the bone defect was bridged with a rigid bone fixation plate that withstood most of the load. Small animal models, such as those of Van der Stok et al. (2013), are easier to use and allow investigation with larger numbers of animals, but they are not representative of the functional and dimensional challenges of scaffolds in large animal models (Hollister et al., 2005). In our study, designing the fixation lugs as direct extensions from the implant body ensured continuity between the cut ends of the bone defect and the implant. Hence, the implant withstood the entire functional load. Moreover, unlike previously reported investigations, our within-subject (contralateral control) experimental design is statistically valuable in large animal models where sample size is often limited due to cost considerations.

The sizing of the implant as well as the design of the mechanical test was based on the assumption of a simple cantilever loading state representing sheep masticatory function. This simplification overlooked the multiaxial nature of the mechanical loading in vivo as well as possible transient peak forces applied to the reconstructed mandible in the event of a shock. However, the required reinforcement of the implant to avert hardware failure in such cases would be opposed to the finding of our study, which demonstrated that lower stiffness scaffolds better promote bone ingrowth. The aim of the mechanical test was to characterize the behavior of the reconstructed mandibles after a 12-week bone-healing

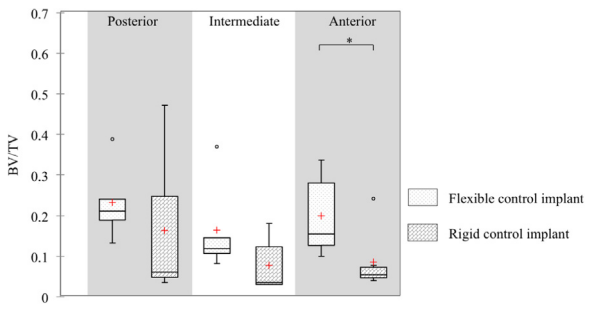

Fig. 15 – BV/TV of group A versus group B control implants in the three longitudinal thirds (sub-volumes P, I and A) (red crosses are the means, $^{*}p < 0.05$). (For interpretation of the references to color in this figure legend, the reader is referred to the web version of this article.)

period. By comparison, several other mechanical test types have been used to assess the stiffness of bone–implant constructs using porous titanium implants. Van der Stok et al. (2013) reported on a 3-point bending test to assess reconstructed femurs in their rodent model. Wieding et al. (2015) used torsional testing to assess the mechanical properties of implanted sheep metatarsal bones. We suggest that the cantilever bending test used in our study is reasonably representative of the physiological loading of the lower jaw and is more appropriate than other loading regimes in our case due the changing cross section of the bone tested. Moreover, it is associated with minimal stress concentration (Abu-Serriah et al., 2005).

Formaldehyde fixation could potentially affect the outcome of the mechanical testing, however the tests were intended to assess the overall behavior of the reconstructed mandibles comparatively rather than as a mechanical characterization of the newly formed bone tissue. Moreover, it has been shown that formaldehyde fixation has only a minor impact on the Young's modulus of bone in bending (Currey et al., 1995).

Interestingly, the results of the mechanical testing suggested incomplete bone healing of the anterior interface in group A. This was not the case for the hemi-mandibles equipped with flexible implants (group B) where the anterior interface had been bridged with bone despite a number of implant lug fractures occurring. This suggests satisfactory bone ingrowth at the interfaces when the reconstruction does not create strong discontinuities in rigidity along the main axis of the bone. This supports our primary hypothesis stating that reduced overall stiffness of the porous implant promotes bone ingrowth. The hardware failures encountered during the healing period, be they screw loosening or implant lug damage, could impair the validity of our findings. We were not able to date the occurrence of hardware failure during the post-implantation period as no intermediate radiological assessment was included in our study. However, bone colonization of the flexible implant interfaces as well as the uneventful bone-healing period for most ewes (5/6) suggests that fractures may have occurred relatively late during the 12 week survival period. Weight gain was recorded during the healing period, also indicating good recovery and that the implanted mandibles were compatible with oral feeding. Furthermore, as Table 1 illustrates, each group showed consistent and specific patterns of hardware failure, which were the same for the porous and control sides in each group. It must be recalled that the implant fixation lugs and screws were identical for both rigid (group A) and flexible (group B) implants. This reveals clearly different loading response of the implant-bone constructs relative to the stiffness of the implant during the healing period, as confirmed through mechanical testing and micro-CT assessment for flexible implants.

The favorable bony ingrowth of the porous implants compared with the control in our study is consistent with previously reported results evaluating bone ingrowth of implants positioned in critical-size defects in animal models (Van der Stok et al., 2013; Wieding et al., 2015; Ponader et al., 2010). We used a stringent micro-CT BV/TV assessment method comparable to that reported by Van der Stok et al.

(2013). This micro-CT post-treatment method allowed us to measure the volume of bone tissue recruited into the pores of the implant. Even in the worst-case scenario (accounting for potential artifact in the BV/TV calculation), our micro-CT findings were confirmed for flexible implants. Wieding et al. (2015), for instance, identified the newly formed bone within the bone defect zone using Hounsfield Unit threshold ranges on clinical CT-scan images. This method did not allow assessment of the content of the implant pores and it was not adjusted for titanium-related artifacts. Other methods based on Boolean subtraction of titanium volume have been proposed to calculate newly formed bone volumes within the implant using finite element models matched on micro-CT images, but such approaches have not addressed the artifact issue (Muraru et al., 2009; Van Cleynenbreugel et al., 2006).

The confounding factor related to the differences in TV (total available volume for bony ingrowth) between porous and control implants could not be eliminated, neither in our study nor in those prior. However, this confounding factor could not be suspected of having played a role in the comparison of rigid *vs* flexible implants, where the differences in TV are negligible since both implants are based on the same porous design. Moreover, this effect would be expected to be detrimental for flexible implants where the connecting longitudinal struts are missing, which marginally increases TV. The superior performance of flexible implants in terms of bone formation found in our study confirms the results of Wieding et al.'s (2015) work, though their implants were not in themselves load-bearing. The incomplete loading of the porous implants because of additional rigid fixation of the bone defect likely explains the absence of significant differences between the two types of implants tested by Van der Stok et al. (2013).

The basic design of our flexible implant was dictated by the expected primary flexural loading of the implant in this anatomical site and by the requirement of mechanically identical (from an overall stiffness perspective) implants for our within-subject study. The drawback of this lateral beam design is the heterogeneity of stress distribution among the pores of the flexible implant compared with the rigid. On the other hand, the design can easily be adapted to the estimated loading for other studies or anatomical sites. It could also form the basis of an approach to develop personalized implants for clinical use, taking into account individual anatomical and physiological parameters of the receiving patient. In accordance with our primary hypothesis stating that bone ingrowth would depend on the local strain of the implant mesh, deliberate moderate 'undersizing' of the implant stiffness could be desirable for clinical use since the loading could be controlled and the reconstructed bone defect gradually functionalized resulting in superior bone ingrowth.

5. Conclusion

This crossover animal study confirmed that (1) fully load-bearing titanium porous implants allow for better bone ingrowth of critical-size mandibular bone defects in adult ewes than empty implants exhibiting identical overall mechanical stiffness, and (2) that reducing the overall stiffness of the porous implant by an order of magnitude promotes superior bone formation compared to more rigid implants.

Acknowledgments

The authors are very grateful to the "Fondation des Gueules Cassées" (Grant no. 36-2012) and the "Fondation de l'Avenir" (Grant no. ETO-575) for their financial support, to Prof. Ph. Menasché, head of the "Laboratoire de Recherches Biochirurgicales – Fondation Alain Carpentier", and to Ms. J. Piquet, Ms. M. Rancic and Mr. A. Lalo for hosting the animal experiment in their facilities and for providing highest-standard animal care.

REFERENCES

Abu-Serriah, M., Kontaxis, A., Ayoub, A., Harrison, J., Odell, E., Barbenel, J., 2005. Mechanical evaluation of mandibular defects reconstructed using osteogenic protein-1 (rhOP-1) in a sheep model: a critical analysis. Int. J. Oral Maxillofac. Surg. 34 (3), 287–293.

Barbas, A., Bonnet, A.-S., Lipinski, P., Pesci, R., Dubois, G., 2012. Development and mechanical characterization of porous titanium bone substitutes. J. Mech. Behav. Biomed. Mater. 9, 34–44.

Bell, R.B., Weimer, K.A., Dierks, E.J., Buehler, M., Lubek, J.E., 2011. Computer planning and intraoperative navigation for palatomaxillary and mandibular reconstruction with fibular free flaps. J. Oral Maxillofac. Surg. 69 (3), 724–732.

Catalá-Lehnen, P., Rendenbach, C., Heiland, M., Khakpour, P., Rueger, J.M., Schmelzle, R., et al., 2012. Long-term donor-site morbidity after microsurgical fibular graft: is there a difference between the medial approach and the lateral approach?. J. Oral Maxillofac. Surg. J. Am. Assoc. Oral Maxillofac. Surg. 70 (9), 2198–2204.

Currey, J.D., Brear, K., Zioupos, P., Reilly, G.C., 1995. Effect of formaldehyde fixation on some mechanical properties of bovine bone. Biomaterials 16 (16), 1267–1271.

De Wild, M., Schumacher, R., Mayer, K., Schkommodau, E., Thoma, D., Bredell, M., et al., 2013. Bone regeneration by the osteoconductivity of porous titanium implants manufactured by selective laser melting: a histological and micro computed tomography study in the rabbit. Tissue Eng. A. 19 (23–24), 2645–2654.

Drosos, G.I., Babourda, E., Magnissalis, E.A., Giatromanolaki, A., Kazakos, K., Verettas, D.A., 2012. Mechanical characterization of bone graft substitute ceramic cements. Injury 43 (3), 266–271.

Faria, P.E.P., Carvalho, A.L., Felipucci, D.N.B., Wen, C., Sennerby, L., Salata, L.A., 2010. Bone formation following implantation of titanium sponge rods into humeral osteotomies in dogs: a histological and histometrical study. Clin. Implant. Dent. Relat. Res. 12 (1), 72–79.

Foster, R.D., Anthony, J.P., Sharma, A., Pogrel, M.A., 1999. Vascularized bone flaps versus nonvascularized bone grafts for mandibular reconstruction: an outcome analysis of primary bony union and endosseous implant success. Head Neck 21 (1), 66–71.

Fujibayashi, S., Neo, M., Kim, H.-M., Kokubo, T., Nakamura, T., 2004. Osteoinduction of porous bioactive titanium metal. Biomaterials 25 (3), 443–450.

Goh, B.T., Lee, S., Tideman, H., Stoelinga, P.J.W., 2008. Mandibular reconstruction in adults: a review. Int. J. Oral Maxillofac. Surg. 37 (7), 597–605.
He, G., Liu, P., Tan, Q., 2012. Porous titanium materials with entangled wire structure for load-bearing biomedical applications. J. Mech. Behav. Biomed. Mater. 5 (1), 16–31.
He, G., Liu, P., Tan, Q., Jiang, G., 2013. Flexural and compressive mechanical behaviors of the porous titanium materials with entangled wire structure at different sintering conditions for load-bearing biomedical applications. J. Mech. Behav. Biomed. Mater. 28, 309–319.
Hirsch, D.L., Garfein, E.S., Christensen, A.M., Weimer, K.A., Saddeh, P.B., Levine, J.P., 2009. Use of computer-aided design and computer-aided manufacturing to produce orthognathically ideal surgical outcomes: a paradigm shift in head and neck reconstruction. J. Oral Maxillofac. Surg. 67 (10), 2115–2122.
Hollister, S., Lin, C., Saito, E., Lin, C., Schek, R., Taboas, J., et al., 2005. Engineering craniofacial scaffolds. Orthod. Craniofac. Res. 8 (3), 162–173.
Karageorgiou, V., Kaplan, D., 2005. Porosity of 3D biomaterial scaffolds and osteogenesis. Biomaterials 26 (27), 5474–5491.
Kerrary, S., Schouman, T., Cox, A., Bertolus, C., Febrer, G., Bertrand, J.C., 2011. Acute compartment syndrome following fibula flap harvest for mandibular reconstruction. J. Cranio-Maxillo-Fac. Surg. Publ. Eur. Assoc. Cranio-Maxillo-Fac. Surg. 39 (3), 206–208.
Lopez-Heredia, M.A., Sohier, J., Gaillard, C., Quillard, S., Dorget, M., Layrolle, P., 2008. Rapid prototyped porous titanium coated with calcium phosphate as a scaffold for bone tissue engineering. Biomaterials 29 (17), 2608–2615.
Marin, E., Pressacco, M., Fusi, S., Lanzutti, A., Turchet, S., Fedrizzi, L., 2013. Characterization of grade 2 commercially pure trabecular titanium structures. Mater. Sci. Eng. C 33 (5), 2648–2656.
Mehta, R.P., Deschler, D.G., 2004. Mandibular reconstruction in 2004: an analysis of different techniques. Curr. Opin. Otolaryngol. Head Neck Surg. 12 (4), 288–293.
Momoh, A.O., Yu, P., Skoracki, R.J., Liu, S., Feng, L., Hanasono, M. M., 2011. A prospective cohort study of fibula free flap donor-site morbidity in 157 consecutive patients. Plast. Reconstr. Surg. 128 (3), 714–720.
Muraru, L., Van Lierde, C., Naert, I., Vander Sloten, J., Jaecques, S. V.N., 2009. Three-dimensional finite element models based on in vivo microfocus computed tomography: elimination of metal artefacts in a small laboratory animal model by registration with artefact-free reference images. Adv. Eng. Softw. 40 (11), 1207–1210.
Myeroff, C., Archdeacon, M., 2011. Autogenous bone graft: donor sites and techniques. J. Bone Jt. Surg. 93 (23), 2227–2236.
Niinomi, M., Nakai, M., 2011. Titanium-based biomaterials for preventing stress shielding between implant devices and bone. Int. J. Biomater., e836587 2011 Jun 22.
Oh, I.-H., Nomura, N., Masahashi, N., Hanada, S., 2003. Mechanical properties of porous titanium compacts prepared by powder sintering. Scr. Mater. 49 (12), 1197–1202.
Otawa, N., Sumida, T., Kitagaki, H., Sasaki, K., Fujibayashi, S., Takemoto, M., et al., 2015. Custom-made titanium devices as membranes for bone augmentation in implant treatment: Modeling accuracy of titanium products constructed with selective laser melting. J. Cranio-Maxillofac. Surg. 43 (7), 1289–1295.
Otsuki, B., Takemoto, M., Fujibayashi, S., Neo, M., Kokubo, T., Nakamura, T., 2006. Pore throat size and connectivity determine bone and tissue ingrowth into porous implants: three-dimensional micro-CT based structural analyses of porous bioactive titanium implants. Biomaterials 27 (35), 5892–5900.
Palmquist, A., Snis, A., Emanuelsson, L., Browne, M., Thomsen, P., 2013. Long-term biocompatibility and osseointegration of electron beam melted, free-form-fabricated solid and porous titanium alloy: experimental studies in sheep. J. Biomater. Appl. 27 (8), 1003–1016.
Ponader, S., von Wilmowsky, C., Widenmayer, M., Lutz, R., Heinl, P., Körner, C., et al., 2010. In vivo performance of selective electron beam-melted Ti-6Al-4V structures. J. Biomed. Mater. Res. A 92A (1), 56–62.
Schouman, T., Khonsari, R.H., Goudot, P., 2015. Shaping the fibula without fumbling: the SynpliciTi customised guide-plate. Br. J. Oral. Maxillofac. Surg. 53 (5), 472–473.
St-Pierre, J.-P., Gauthier, M., Lefebvre, L.-P., Tabrizian, M., 2005. Three-dimensional growth of differentiating MC3T3-E1 pre-osteoblasts on porous titanium scaffolds. Biomaterials 26 (35), 7319–7328.
Takemoto, M., Fujibayashi, S., Neo, M., Suzuki, J., Kokubo, T., Nakamura, T., 2005. Mechanical properties and osteoconductivity of porous bioactive titanium. Biomaterials 26 (30), 6014–6023.
Van Cleynenbreugel, T., Schrooten, J., Van Oosterwyck, H., Vander Sloten, J., 2006. Micro-CT-based screening of biomechanical and structural properties of bone tissue engineering scaffolds. Med. Biol. Eng. Comput. 44 (7), 517–525.
Van der Stok, J., Van der Jagt, O.P., Amin Yavari, S., De Haas, M.F.P., Waarsing, J.H., Jahr, H., et al., 2013. Selective laser melting-produced porous titanium scaffolds regenerate bone in critical size cortical bone defects. J. Orthop. Res. Publ. Orthop. Res. Soc. 31 (5), 792–799.
Vehof, J.W., Spauwen, P.H., Jansen, J.A., 2000. Bone formation in calcium-phosphate-coated titanium mesh. Biomaterials 21 (19), 2003–2009.
Vehof, J.W., Mahmood, J., Takita, H., van't Hof, M.A., Kuboki, Y., Spauwen, P.H., et al., 2001. Ectopic bone formation in titanium mesh loaded with bone morphogenetic protein and coated with calcium phosphate. Plast. Reconstr. Surg. 108 (2), 434–443.
Warnke, P.H., Douglas, T., Wollny, P., Sherry, E., Steiner, M., Galonska, S., et al., 2009. Rapid prototyping: porous titanium alloy scaffolds produced by selective laser melting for bone tissue engineering. Tissue Eng. C Methods 15 (2), 115–124.
Wieding, J., Lindner, T., Bergschmidt, P., Bader, R., 2015. Biomechanical stability of novel mechanically adapted open-porous titanium scaffolds in metatarsal bone defects of sheep. Biomaterials 46, 35–47.
Xue, W., Krishna, B.V., Bandyopadhyay, A., Bose, S., 2007. Processing and biocompatibility evaluation of laser processed porous titanium. Acta Biomater. 3 (6), 1007–1018.